Bull. Mater. Sci., Vol. 37, No. 1, February 2014, pp. 53–60. © Indian Academy of Sciences.

Effect of copper doping on structural, optical and electrical properties of $Cd_{0.8}Zn_{0.2}S$ films prepared by chemical bath deposition

K HADASA, G YELLAIAH and M NAGABHUSHANAM*
Department of Physics, University College of Science, Osmania University, Hyderabad 500 007, India

MS received 18 November 2012; revised 6 March 2013

Abstract. **$Cd_{0.8}Zn_{0.2}S$:Cu films of 1·3–6·1 mole percentage of copper have been grown on mica substrate by using chemical bath deposition technique. The films have been characterized by using XRD, SEM and UV spectrophotometer. X-ray diffraction studies have shown that the films are polycrystalline. The average crystallite size as measured from XRD data is in the range of 125–130 nm. The activation energies of $Cd_{0.8}Zn_{0.2}S$:Cu films, as observed from d.c. conductivity studies in the temperature range (77–300 K) studied, decreased with the increase in Cu concentration. The optical absorption studies have revealed that the energy gap increases gradually with an increase in Cu concentration, whereas conductivity studies have shown an anomalous increase in conductivity in films of 3·8 mole percentage of Cu. SEM pictures have revealed the presence of defects with spherical structure having fibre network. The variation of electrical conductivity is explained based on the defects present and by adopting tunneling mechanism.**

Keywords. **Ternary semiconductor compounds; CBD method; structural properties; optical and electrical studies.**

1. Introduction

Study of $Cd_{(1-x)}Zn_xS$ compound semiconductors has attracted academicians and technologists because, their energy gap can be tuned and the lattice parameters can be varied suitably with the variation of x. In recent years, the replacement of CdS with its ternary alloy, $Cd_{(1-x)}Zn_xS$, has been attempted for the improvement of $(Cd, Zn)S/Cu(In, Ga)Se_2$ solar cell performance, this has resulted in a higher energy conversion efficiency of 19·52% (Bhattacharya *et al* 2006). Moreover, replacements of CdS with higher energy gap ternary $Cd_{(1-x)}Zn_xS$ compound has also led to a decrease in window absorption loss and has resulted in an increase in the short circuit current in the solar cell. Thin films of CdZnS have also been proved to be equally useful in the fabrication of solar cells. These films are prepared by several techniques like CVD (Ma *et al* 2007), MOCVD (Chu *et al* 1991), Sputtering (Abouelfotouh *et al* 1979), spray pyrolysis (Ma and Bube 1977; Kwook and Siu 1979; Kwook 1980), electrodeposition (Al bassan 1999), successive ionic layer adsorption and reaction (SILAR) (Shrivastava and Verma 2007) etc. All these techniques are highly sophisticated and at the same time expensive. Therefore, work has been continued to find out ways to prepare films by simple methods so as to reduce cost of solar cell.

Chemical bath deposition (CBD) (Chopra *et al* 1982) is a thin film technique, identified in the past decade, by which compound semiconductor thin films of typically 0·02–1 μm thickness can be deposited on substrates placed in contact with dilute baths containing metal ions and a source of sulphide or selenide ions. Many I–VI, II–VI, IV–VI and V–VI semiconductors are included in the list of materials deposited by this technique (Lokhande 1991; Nair *et al* 1998). CBD is one of the most convenient, reliable, simplest and less expensive methods used to prepare films at close to room temperature having large area industrial applications. The technique of CBD involves controlled precipitation from solution of a compound on a suitable substrate. The technique offers many advantages over the more established vapour phase synthetic routes to semiconductor materials, such as CVD, MBE and spray pyrolysis. Factors such as control of film thickness and deposition rate by varying the solution pH, temperature and reagent concentration are allied with the ability of CBD to coat large areas in a reproducible and low cost process. Another advantage of CBD method with respect to other methods is that the films can be deposited on different kinds, shapes and sizes of substrates (Kale and Lokhande 2005; Barman *et al* 2008).

Many researchers have carried out work on CdZnS films grown by CBD (Padam *et al* 1988; Dona and Herrero 1995; Yamaguchi *et al* 1996; Lee *et al* 2003; Oladeji and Chow 2005; Song *et al* 2005; Borse *et al* 2006; Chavhan *et al* 2008; Sanap and Pawar 2011; Mahidi and Ali-Ani 2012) and other sophisticated methods on glass slides but not on copper doped CdZnS films grown on mica substrate. Therefore, an attempt has been made for the first time to grow $Cd_{0.8}Zn_{0.2}S$ films doped with different concentrations of copper on mica

*Author for correspondence (mamidala_nb@yahoo.com)

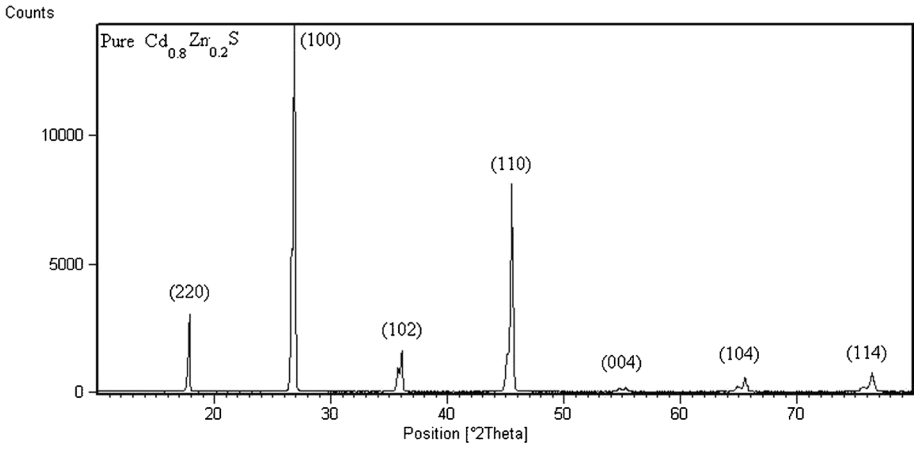

Figure 1. XRD pattern of $Cd_{0·8}Zn_{0·2}S$ thin film grown on mica substrate.

Table 1. Comparison of the observed XRD data with ICDD–JCPDS data.

ICDD–JCPDS data of $Cd_{0·8}Zn_{0·2}S$ (H) (PDF No. 400835)				Observed X-ray diffraction data of pure $Cd_{0·8}Zn_{0·2}S$			Observed X-ray diffraction data of Cu(2·5 mole%) doped $Cd_{0·8}Zn_{0·2}S$		
2θ	I	hkl	d(nm)	2θ	I	d(nm)	2θ	I	d(nm)
				17·819	18	0·498	17·803	20	0·498
25·522	51	100	0·349	26·576	34	0·335	26·576	43	0·335
27·103	100	002	0·329	26·852	100	0·332	26·841	100	0·332
28·799	43	101	0·309	28·708	0·05	0·311			
37·311	18	102	0·241	36·060	11	0·249	36·062	10	0·249
44·870	61	110	0·202	45·508	57	0·199	45·510	45	0·199
55·744	4	004	0·165	55·280	1	0·166	55·271	1	0·166

substrate by chemical bath deposition technique. Thickness of the films was varied by varying deposition time. Structural, optical and electrical properties of these films have been analysed using XRD, SEM, UV-spectrophotometer, d.c. electrical conductivity studies and results are reported in this article. The results are explained based on the defects present in the films. The films deposited for 20 min are found to have 334 nm thickness. The studies were made on the films of different thicknesses but the results obtained on $Cd_{0·8}Zn_{0·2}S$:Cu films of 334 nm thickness are presented in this article.

2. Experimental

$Cd_{0·8}Zn_{0·2}S$:Cu films with different concentrations of copper were grown on mica substrate by using chemical-bath deposition method. In this method, equimolar (0·5 M) solutions of cadmium acetate, zinc acetate and thiourea were mixed in definite proportions to yield $Cd_{0·8}Zn_{0·2}S$. $Cd_{0·8}Zn_{0·2}S$ films doped with different concentrations of Cu were obtained by adding different amounts of $CuSO_4$ solution of 0·25 molar concentration to the above solution. The solution was made alkaline by adding 25% of liquid ammonia. Film was grown on a mica substrate by introducing the substrate for a fixed time into the solution mixture maintained at 80(±2)°C. The thickness of the films grown on substrate was varied from 334–869 nm by varying the deposition time ranging from 10–60 min. The films, thus grown, were rinsed in deionized water and were kept for drying in air at room temperature. These films were annealed at 800°C for 1 h in nitrogen atmosphere (0·2 kg/cm^2 pressure). The pressure of the gas was maintained uniformly throughout the sintering process and the furnace was cooled very slowly (1°C /min) to room temperature.

Thickness of the films was measured by interference technique. Structural, optical and electrical studies were carried out on these films using XRD (PHILIPS- PAN ANALYTICAL X'PERT PLUS), SEM (ZEISS EVO-18), UV-spectrophotometer (SHIMADZU, UV-3100) and a two-probe technique using Keithley 6220 Precision current source and Keithley 182 sensitive digital voltmeter. The diffractograms were recorded with a step size of 0·02°/s (2θ) indicating an accuracy of ±0·02° in the measurement of 2θ.

3. Results and discussion

3.1 *X-ray diffraction studies*

Figure 1 shows XRD pattern of an undoped $Cd_{0·8}Zn_{0·2}S$ film of nearly 334 nm thickness grown on mica substrate.

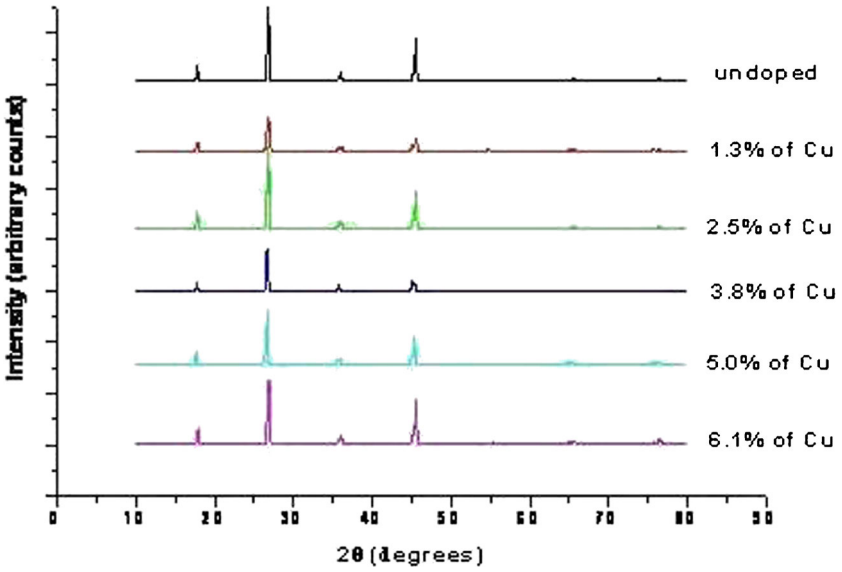

Figure 2. XRD graphs of $Cd_{0·8}Zn_{0·2}S$ films doped with different concentrations of Cu of thickness 334 nm.

The figure consists of sharp peaks indicating that the film is polycrystalline. To identify structure of the films, observed diffraction peak positions and their intensities were compared with the standard ICDD–JCPDS data of $Cd_{0·8}Zn_{0·2}S$ (cubic) and $Cd_{0·8}Zn_{0·2}S$ (hexagonal) structures and found to match (within the experimental limitations) with those of $Cd_{0·8}Zn_{0·2}S$ (hexagonal) structure (PDF No. 400835) and their values are shown in table 1. The observed peaks are assigned with appropriate miller indices (table 1) by comparing the reported and observed d values. The lattice parameters were computed using the above data as $a = 0·282$ nm and $c = 0·664$ nm.

Figure 2 shows XRD patterns of various Cu-doped $Cd_{0·8}Zn_{0·2}S$ films. It is observed from these diffraction patterns that $Cd_{0·8}Zn_{0·2}S$:Cu films also have polycrystalline nature and have almost similar peaks as compared to undoped $Cd_{0·8}Zn_{0·2}S$ film. The observed data is again compared with ICDD–JCPDS data (PDF No. 400835) and found that all Cu-doped $Cd_{0·8}Zn_{0·2}S$ films possess hexagonal structure. Further, it is observed that $Cd_{0·8}Zn_{0·2}S$ films of different thicknesses and doping concentrations have similar structure (hexagonal).

The lattice parameters a and c are also calculated for all the films of different mole percentages of Cu and are shown in table 2. For the sake of comparison, the lattice parameters obtained in pure $Cd_{0·8}Zn_{0·2}S$ are also given in table 2.

From the above table, it can be clearly seen that the lattice parameters of undoped and doped films are almost the same which means that within the limited doping concentration of Cu, i.e. between 0 and 6·1 mole% in $Cd_{0·8}Zn_{0·2}S$ film, did not affect crystal structure of $Cd_{0·8}Zn_{0·2}S$.

Table 2. Calculated lattice parameters from XRD data in $Cd_{0·8}Zn_{0·2}S$:Cu films.

Sl. No	Mole% of Cu	Lattice parameters	
		a(nm)	c(nm)
1.	Undoped	0·282	0·664
2.	1·3	0·279	0·654
3.	2·5	0·282	0·664
4.	3·8	0·283	0·669
5.	5·0	0·283	0·668
6.	6·1	0·282	0·663

For all the samples, an average crystallite size has been determined from XRD data using Debye–Scherrer formula:

$$\tau = K\lambda/\beta\cos\theta,$$

where K is a constant taken to be 0·94, λ the wavelength of X-ray used (0·154 nm), β the FWHM of the peak and θ the Bragg's angle.

It is found that the average crystallite size in all these films has been in the range of 125–130 nm, more precisely about 128 nm.

3.2 *SEM studies*

Figure 3 shows scanning electron micrographs of undoped and Cu-doped $Cd_{0·8}Zn_{0·2}S$ films. From the micrographs, it is clear that (i) spheres with fibre net structures are observed in

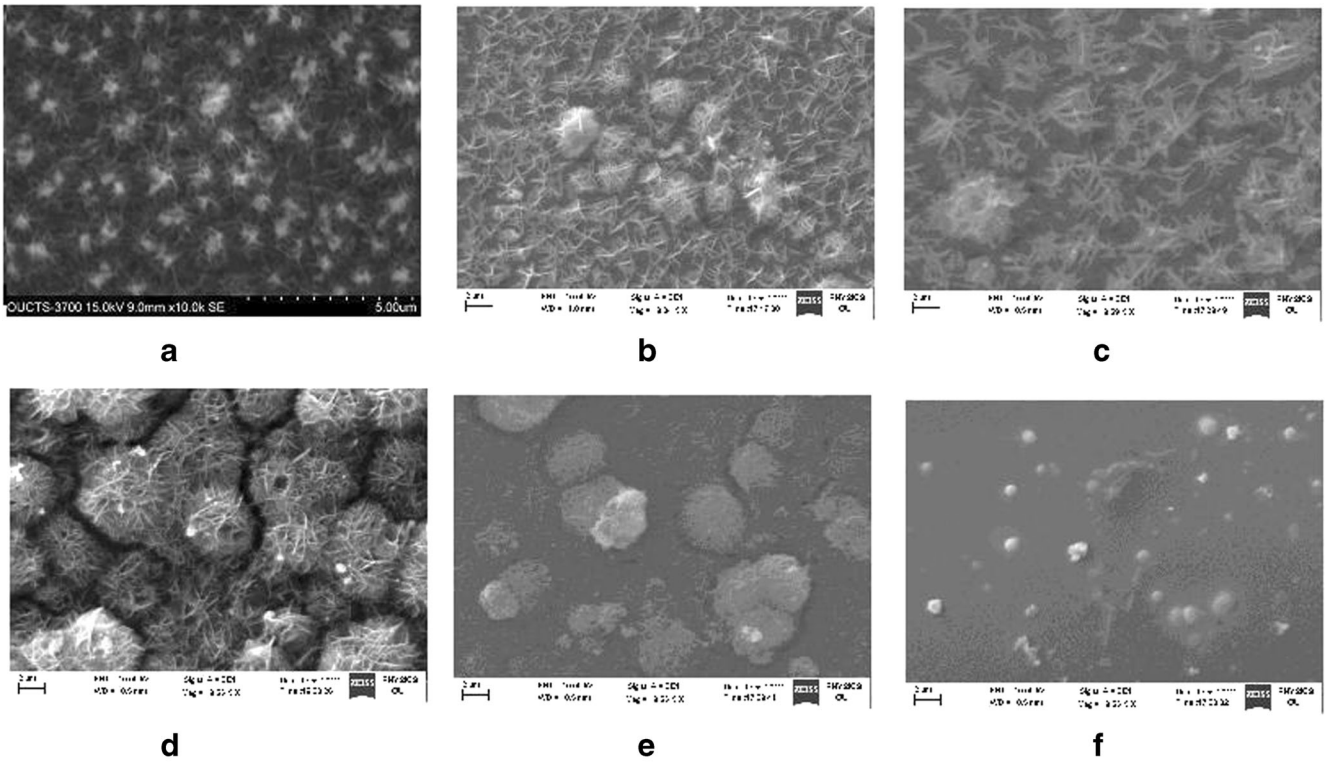

Figure 3. SEM of (**a**) $Cd_{0.8}Zn_{0.2}S$ (undoped), (**b**) $Cd_{0.8}Zn_{0.2}S$ (1·3 mole% of Cu), (**c**) $Cd_{0.8}Zn_{0.2}S$ (2·5 mole% of Cu), (**d**) $Cd_{0.8}Zn_{0.2}S$ (3·8 mole% of Cu), (**e**) $Cd_{0.8}Zn_{0.2}S$ (5·0 mole% of Cu) and (**f**) $Cd_{0.8}Zn_{0.2}S$ (6·1 mole% of Cu).

Table 3. EDAX data of undoped and doped $Cd_{0.8}Zn_{0.2}S$:Cu films.

Sl. No	$Cd_{0.8}Zn_{0.2}S + Cu$ [Mole%]	Element (wt%)					
		C	S	Cu	Zn	Cd	O
1.	$Cd_{0.8}Zn_{0.2}S$+Cu[0%]	5·33	45·40	–	8·48	38·72	2·07
2.	$Cd_{0.8}Zn_{0.2}S$+Cu[1·3%]	3·80	43·47	1·00	8·46	40·58	2·69
3.	$Cd_{0.8}Zn_{0.2}S$+Cu[2·5%]	–	47·86	1·95	8·65	40·10	1·44
4.	$Cd_{0.8}Zn_{0.2}S$+Cu[3·8%]	–	48·44	2·06	7·73	39·70	2·07
5.	$Cd_{0.8}Zn_{0.2}S$+Cu[5%]	–	46·42	4·11	8·10	39·74	1·63
6.	$Cd_{0.8}Zn_{0.2}S$+Cu[6·1%]	–	46·46	5·94	7·66	38·8	1·14

the deposited $Cd_{0.8}Zn_{0.2}S$:Cu films and (ii) size of the sphere increases initially with the increase in Cu concentration and it is dissolved gradually into the structure on further increase of dopant concentration.

Such fibrous films may be useful for gas sensing applications.

3.3 *EDAX studies*

From table 3, the compositional data of EDAX confirms nearly nominal composition of the synthesized $Cd_{0.8}Zn_{0.2}S$:Cu films.

3.4 *Optical absorption studies*

Figure 4 shows variation of absorbance of $Cd_{0.8}Zn_{0.2}S$:Cu films with frequency at room temperature in the wavelength region 200–800 nm. The absorption edge shift is towards UV region for concentration of Cu and later shift is not so significant. The high absorbance in UV region (350–450 nm) make the films suitable for window layers of solar cells and other photovoltaic devices.

The optical absorption coefficient (α) near the absorption edge is evaluated from the equation:

$$\alpha(\nu) = 2{\cdot}303\frac{A}{d},$$

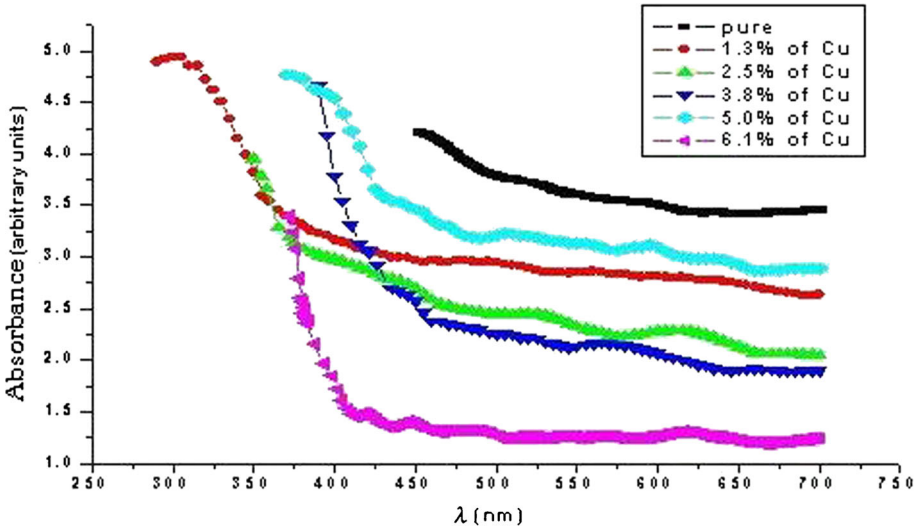

Figure 4. Absorbance of $Cd_{0.8}Zn_{0.2}S$:Cu films of 334 nm thickness.

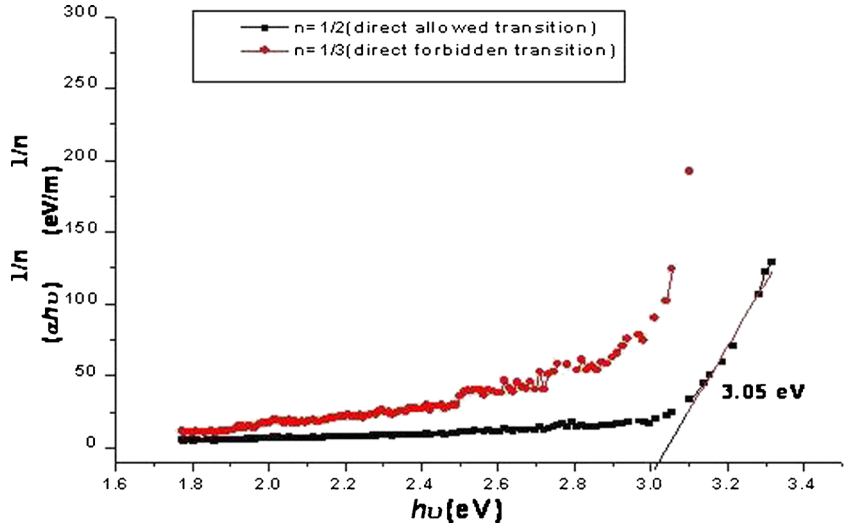

Figure 5. A plot of $(\alpha h\nu)^{1/n}$ vs $h\nu$ of $Cd_{0.8}Zn_{0.2}S$ film (334 nm thickness) doped with 6·1 mole% of Cu.

where d is the thickness of each sample and A the absorption, respectively. The optical absorption of semiconductor materials, above the exponential tail, follows a power law given by Mott and Davis (1979) which is in the most general form:

$$\alpha(\upsilon) = \frac{C(h\nu - E_{\text{opt}})^n}{h\nu},$$

where C is an energy-independent constant (band edge steepness parameter in Tauc's picture), n takes values of 1/2, 2, 1/3, 3 for direct-allowed, indirect-allowed, direct-forbidden and indirect-forbidden transitions, respectively. As CdZnS is a direct bandgap material, $n = 1/2$ for the allowed transition. The bandgap has been calculated by extrapolating the linear region of the plot $(\alpha h\nu)^2$ vs $h\nu$ on the energy axis as shown in figure 5.

In order to understand the possibility of occurrence of direct allowed/forbidden transitions in the film, graphs can be drawn between $(\alpha h\nu)^{1/n}$ vs $h\nu$ for $n = 1/2$ and 1/3. However, as shown in figure 5, variations corresponding to direct-allowed and direct-forbidden transitions are seen clearly with lower transition energy value in case of direct-forbidden than direct-allowed transitions. This gives a way to think about the possible reasons for the forbidden transitions. Camassel *et al* (1979) studied the forbidden transitions in TiO_2 and forbidden transitions are accounted by them to stress induced breaking of the selection rules. Henneberger *et al* (1974), while studying the interband con-

Table 4. Energy gap values obtained from optical absorption studies of $Cd_{0.8}Zn_{0.2}S$:Cu films.

Sl. No.	Mole% of Cu	Energy gap (eV)
1.	Undoped	2·66
2.	1·3	2·95
3.	2·5	2·86
4.	3·8	3·03
5.	5·0	2·94
6.	6·1	3·05

ductivity for forbidden transitions have also found that the forbidden transitions lead to conductivity roughly hundred times smaller than the allowed transitions and is due to the tunneling of charge carriers. In view of these results, it appears that the stresses induced by the spherical defects (ball-like structures evidenced from SEM pictures) cause tunneling conductivity surpassing spectroscopic selection rules.

The direct energy gap of $Cd_{0.8}Zn_{0.2}S$ film has been calculated and found to be 2·66 eV, which matches with E_g (2·62 eV) value obtained by Pawan Kumar *et al* (2004) and E_g (2·59 eV) value obtained by Xia *et al* (2011).

The direct energy gap of all the films of different concentrations of Cu, calculated in a similar way, are shown in table 4 and the graphical variation in figure 6. The graph indicates that E_g value increases rapidly at low concentrations of Cu and it reaches more or less a saturation value at higher concentrations which means that the influence of defects created by Cu dopants at lower concentration is more rather than at higher concentration. Fibre-like structured defects were also observed earlier by Sanap and Pawar (2011) in $Cd_{(1-x)}Zn_xS$ thin films consisting of higher concentration of Zn ($x = 0{\cdot}8$). The present study leads to infer that the copper dopant might interact more with Zn ions, though its concentration is low ($x = 0{\cdot}2$) and helps in the formation of fibre networked spherical defects. However, the same dopant (Cu) causes the dissociation of such defects into smaller ones as the concentration increases.

SEM pictures have revealed the presence of clusters in the form of spherical nature wound with fibre network at lower concentrations of Cu, which might be influencing the lattice structure. At higher concentrations of doping (6·1 mole%), more number of such clusters with larger size could be expected but SEM pictures taken on higher doping concentrations do not reveal such networked defects. The disappearance of defects may be due to dissociation into smaller size and getting dispersed into the lattice leading to a saturation value of direct energy gap. Thus, the rise of E_g observed at lower concentration is not seen at higher concentrations. Such wider bandgap of the deposited films make them suitable for optoelectronic devices like window layers in solar cells.

Though the solubility product of CuS($k_{sp} = 6 \times 10^{-37}$) is much lower than the solubility product of CdS($k_{sp} = 8 \times 10^{-27}$) or ZnS($k_{sp} = 2 \times 10^{-25}$), the present results support

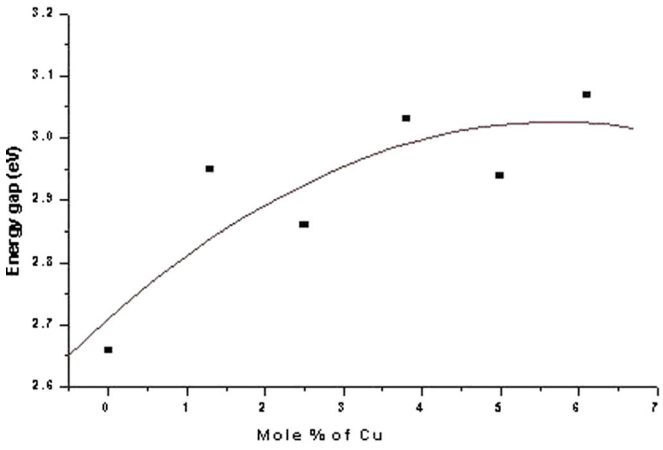

Figure 6. Energy gap vs mole% of Cu in $Cd_{0.8}Zn_{0.2}S$ films.

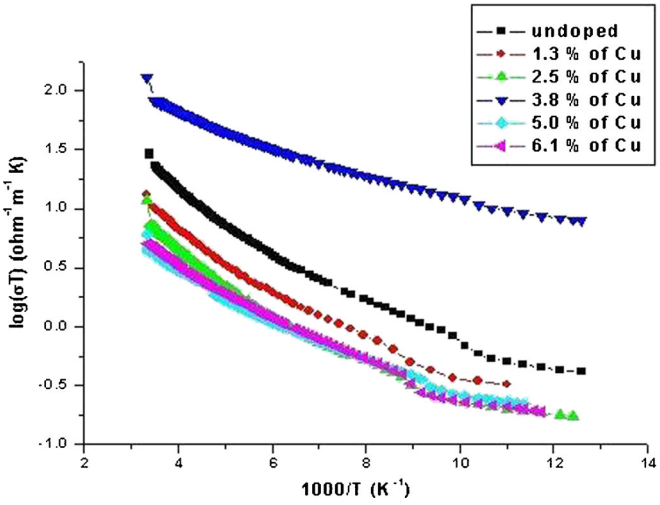

Figure 7. d.c. conductivity vs temperature (77–300 K) graph of undoped and Cu-doped $Cd_{0.8}Zn_{0.2}S$ films of thickness 334 nm.

that Cu is getting into the lattice, reaching the defect site and causing changes in the optical and electrical properties. XRD pattern also supports absence of CuS in the film, thereby less solubility product of CuS will not cause in the way of defect formation as the doping concentration is very low.

3.5 *Electrical conductivity studies*

Variation of electrical conductivity with temperature was studied on pure and Cu doped $Cd_{0.8}Zn_{0.2}S$ films annealed at 800 °C for 1 h in nitrogen gas atmosphere. The $\log(\sigma T)$ variation with temperature (T) is shown in figure 7. These graphs show clearly that the conductivity decreases with decrease in temperature and at a given temperature the conductivity decreases with increase in mole percentage of Cu till 2·5 mole% and then it increases at 3·8 mole% and again it decreases with further increase in mole% of Cu. This type of variation in conductivity may be due to the replacement of

Table 5. Activation energies calculated at low temperature region for $Cd_{0·8}Zn_{0·2}S$:Cu films of thickness, 334 nm.

Sl. No.	Mole% of Cu	Activation energy (meV)
1.	Undoped	10·7
2.	1·3	12·0
3.	2·5	12·3
4.	3·8	9·7
5.	5·0	12·3
6.	6·1	12·5

Cu^{2+} ions in Cd^{2+} and Zn^{2+} vacancies at the beginning and formation of clusters based with Cu^{2+} interstitial ions along with the ions formed out of other defects like vacancies and interstitial ions. It is obvious that these clusters hinder movement of the charge carriers thereby reducing conduction. The evidence of growth in size of the clusters as observed in 1·3% of Cu-doped crystals (figure 3(b)) will support the argument. However, size of the clusters is observed to decrease but the density of the clusters is found to be more in samples of higher doping concentrations, which means that the clusters are getting dissolved into the matrix at these higher concentrations. The dissolution rate of Cu when compared to that of Zn is more, so the Zn ions may be migrating to surface of the sample and Cu may be replacing Zn, thus causing more mobility to the charge carriers due to which the rise in conductivity may be seen in the films doped with 3·8 % of Cu. Later the higher mobility of the carriers may be allowing the carriers to suppress the excess positive charge accumulated on the surface by means of Zn ion migration, thereby reducing conductivity in higher doping concentrations. The activation energies were also calculated from the extrinsic region of the conductivity variation. The activation energy increases with the increase in Cu concentration and decreases at 3·8 mole% of Cu and later it again increases (table 5). The initial increase in activation energy is due to the formation of Cu clusters with Cd^{2+}/Zn^{2+} vacancies. A drastic decrease in the activation energy of 3·8 mole% of Cu is due to the formation of clusters of large size with fibre network which might be helping in the conduction process. Later the increase in activation energy is due to the increase in density of small-sized clusters by way of fragmentation of bigger clusters and a loss of fibre network.

The optical absorption studies suggest tunneling conductivity in Cu-doped films. Whereas the observed reduction in conductivity may be a resultant effect of increase in energy gap and tunneling effect of charge carriers.

4. Conclusions

(I) The structure of $Cd_{0·8}Zn_{0·2}S$:Cu films is hexagonal for different dopant concentrations.
(II) The crystallite size is almost the same in undoped and copper doped $Cd_{0·8}Zn_{0·2}S$ films.
(III) Cu-doped $Cd_{0·8}Zn_{0·2}S$ films have defects (clusters) of spherical structure with fibre-like linkages.
(IV) Optical bandgap of the films increases with dopant concentration and reaches a saturation value at higher concentrations.
(V) The high electrical conductivity (10^{-2}–$10^{-1}\Omega^{-1}m^{-1}$) in $Cd_{0·8}Zn_{0·2}S$:Cu film with 3·8 mole% of Cu, may be due to its low activation energy because of the formation of clusters of large size with fibre network which may help in conduction process.
(VI) The reduction in conductivity with more than 3·8 mole% of Cu may be a resultant effect of increase in energy gap and tunneling effect of charge carriers as observed from optical absorption studies.

Acknowledgements

The authors thank the Head, Department of Physics, Osmania University, Hyderabad, for his constant encouragement and help while conducting the experimental work.

References

Abouelfotouh F A, Al Awadi R and Abd-Elnaby M M 1979 *Thin Solid Films* **60** 55
Al bassan A A 1999 *Solar Energ. Mater. Sol. C.* **57** 329
Barman J, Borah J P and Sarma K C 2008 *Chalcogenide Lett.* **5** 265
Bhattacharya R N, Contreras M A, Egaas B and Noufi R N 2006 *Appl. Phys. Lett.* **89** 253503
Borse S V, Chavhan S D and Sharma R 2006 *J. Alloys Compds* **436** 407
Camassel J, Pascual J and Mathieu H 1979 *Phys. Rev. B Condensed Matter* **20** 5292
Chavhan S D, Senthilarasu S and Lee S H 2008 *Appl. Surf. Sci.* **254** 4539
Chopra K L, Kainthla R C, Pandya D K and Thakoor A P 1982 *Physics of thin films* (ed.) G Hass *et al* **12** 201
Chu T L, Chu S S, Britt J, Ferekids C and Wu C Q 1991 *J. Appl. Phys.* **70** 2688
Dona J M and Herrero J 1995 *Thin Solid Films* **5** 268
Henneberger K, Strehlow R and Wunsche H J 1974 *Phys. Status Solidi (b)* **61** 455
Kale R B and Lokhande C D 2005 *Appl. Surf. Sci.* **252** 929
Kwook H L and Siu W C 1979 *Thin Solid Films* **61** 249
Kwook H L 1980 *J. Phys. D* **13** 1911
Lee J H, Song W C, Yi J S, Yang K J, Han W D and Hwang J 2003 *Solar Energ. Mater. Solar C.* **431–432** 227
Lokhande C D 1991 *Mater. Chem. Phys.* **27** 1
Ma R M, Wei X L, Dai L, Huo H B and Qin G G 2007 *Nanotechnology* **18** 20
Ma Y Y and Bube R H 1977 *J. Electrochem. Soc. Solid-State Sci. Technol.* **124** 1430
Mahidi M A and Ali-Ani S K J 2012 *Int. J. Nanoelectr. Mater.* **5** 11
Mott N F and Davis E A 1979 *Electronic process in non-cryst. materials*, 165
Nair P K, Nair M T S, Garosia V M and Arenas O L 1998 *Solar Energ. Mater. Sol. C.* **52** 313

Oladeji I O and Chow L 2005 *Thin Solid Films* **474** 77
Padam G K, Malhotra G L and Rao S U M 1988 *J. Appl. Phys.* **63** 770
Pawan Kumar, Misra Aparna, Kumar D, Dharma Neeraj, Sharma T P and Dixit P N 2004 *Opt. Mater.* **27** 261
Sanap V B and Pawar B H 2011 *J. Optoelec. Bio. Mater.* **3** 39
Shrivastava S and Verma B 2007 *Cryst. Res. Technol.* **42** 466
Song J, Li S S, Huang C H, Anderson T J and Crisalle O D 2005 *IEEE Photovoltaic Conf.* 449
Xia Di, Caijuan Tian, Rongzhe Tang, Wei Li, Lianghuan Feng, Jingquan Zhang, Wu Lili and Zhi Lei 2011 *J. Semiconductors* **32** 022003
Yamaguchi T, Yamamoto Y, Tanaka T, Demizu A and Yoshida A 1996 *Thin Solid Films* **281/282** 375